Cite as: Owen *et al.*, *Science* 10.1126/science.abl4784 (2021).

An oral SARS-CoV-2 M^{pro} inhibitor clinical candidate for the treatment of COVID-19

Dafydd R. Owen[1]*, Charlotte M. N. Allerton[1], Annaliesa S. Anderson[2], Lisa Aschenbrenner[3], Melissa Avery[3], Simon Berritt[3], Britton Boras[4], Rhonda D. Cardin[2], Anthony Carlo[3], Karen J. Coffman[3], Alyssa Dantonio[3], Li Di[3], Heather Eng[3], RoseAnn Ferre[4], Ketan S. Gajiwala[4], Scott A. Gibson[5], Samantha E. Greasley[4], Brett L. Hurst[5], Eugene P. Kadar[3], Amit S. Kalgutkar[1], Jack C. Lee[3], Jisun Lee[3], Wei Liu[4], Stephen W. Mason[2]†, Stephen Noell[3], Jonathan J. Novak[3]‡, R. Scott Obach[3], Kevin Ogilvie[3], Nandini C. Patel[1], Martin Pettersson[1]§, Devendra K. Rai[2], Matthew R. Reese[3], Matthew F. Sammons[1], Jean G. Sathish[2], Ravi Shankar P. Singh[1], Claire M. Steppan[3], Al E. Stewart[4], Jamison B. Tuttle[1], Lawrence Updyke[1], Patrick R. Verhoest[1], Liuqing Wei[3], Qingyi Yang[1], Yuao Zhu[2]

[1]Pfizer Worldwide Research, Development & Medical, Cambridge, MA 02139, USA. [2]Pfizer Worldwide Research, Development & Medical, Pearl River, NY 10965, USA. [3]Pfizer Worldwide Research, Development & Medical; Groton, CT 06340, USA. [4]Pfizer Worldwide Research, Development & Medical, La Jolla, CA 92121, USA. [5]Institute for Antiviral Research, Department of Animal, Dairy, and Veterinary Sciences, Utah State University; Logan, UT 84322, USA.

*Corresponding author. Email: Dafydd.owen@pfizer.com

†Present address: Janssen Biopharma; South San Francisco, CA 94080, USA.

‡Present address: Praxis Precision Medicines; Cambridge, MA 02142, USA.

§Present address: GRT Therapeutics; Cambridge, MA 02142, USA.

The worldwide outbreak of coronavirus disease 2019 (COVID-19) caused by severe acute respiratory syndrome coronavirus 2 (SARS-CoV-2) has become a global pandemic. Alongside vaccines, antiviral therapeutics are an important part of the healthcare response to counter the ongoing threat presented by COVID-19. Here, we report the discovery and characterization of PF-07321332, an orally bioavailable SARS-CoV-2 main protease inhibitor with in vitro pan-human coronavirus antiviral activity and excellent off-target selectivity and in vivo safety profiles. PF-07321332 has demonstrated oral activity in a mouse-adapted SARS-CoV-2 model and has achieved oral plasma concentrations exceeding the in vitro antiviral cell potency in a phase I clinical trial in healthy human participants.

Human coronavirus infections are common, with at least four examples (229E, NL63, OC43, HKU1) now considered endemic (*1*).· However, the emergence within the last 20 years of SARS-CoV-1, Middle East Respiratory Syndrome (MERS-CoV) and SARS-CoV-2 as novel human coronaviruses has signaled the significant threat potential of this viral class. The catastrophic SARS-CoV-2 outbreak of 2019 has resulted in 235 million confirmed cases of COVID-19 causing over 4.8 million deaths globally as of October 2021. SARS-CoV-2 is a highly infectious, ribonucleic acid (RNA) beta coronavirus that can cause life-threatening viral pneumonia in the most serious cases. While effective COVID-19 vaccines have been developed within unprecedented timelines, a significant number of people are either unable, due to pre-existing medical conditions, or unwilling to be vaccinated, and global access challenges remain. Limited therapeutic options are available to those who are infected. Oral SARS-CoV-2 specific therapeutics are urgently needed to prevent more severe disease, hospitalization, and death. Treatment may also reduce the period of infectivity. Repurposing of approved drugs in the search for small molecule antiviral agents that target SARS-CoV-2 has thus far been minimally effective (*2*, *3*). Viral RNA-dependent RNA polymerase inhibitors such as molnupiravir and AT-527 are currently undergoing clinical trials for the treatment of COVID-19 (*4*, *5*).

The SARS-CoV-2 genome encodes two polyproteins (pp1a and pp1ab) and four structural proteins (*6*, *7*). The polyproteins are cleaved by the critical SARS-CoV-2 main protease (M^{pro}, also referred to as 3CL protease) at eleven different sites to yield shorter, non-structural proteins vital to viral replication (*8*, *9*). The coronavirus M^{pro} is a three-domain cysteine protease, which features a Cys145-His41 catalytic dyad located in the cleft between domains I and II. Several common features are shared among M^{pro} substrates, including the presence of a Gln residue at P1 (using Schechter-Berger nomenclature (*10*)). No known human cysteine protease cleaves after Gln, thus offering potential selectivity for this viral target over the human proteome (*11*–*13*). Viral proteases are tractable targets for small molecule oral therapies in the treatment of human immunodeficiency (HIV) and hepatitis C (HCV) viruses (*14*, *15*). Moreover, a recent report has demonstrated oral activity of an M^{pro} inhibitor in a transgenic

mouse model of SARS-CoV-2 infection (*16*). Given the pivotal role of SARS-CoV-2 M^{pro} in viral replication, its potential for mechanistic safety, and expected lack of spike protein variant resistance challenges, SARS-CoV-2 M^{pro} inhibition represents an attractive small molecule approach for an oral antiviral therapy to treat COVID-19.

An effort to identify inhibitors of the SARS-CoV-1 M^{pro} in response to the 2002 SARS outbreak led to the identification of PF-00835231 (**1**, Fig. 1) as a potent inhibitor of recombinant SARS-CoV-1 M^{pro} in a fluorescence resonance energy transfer (FRET)-based substrate cleavage assay (*17*). PF-00835231 also demonstrated potent inhibition (inhibition constant (K_i) = 0.271 nM) of recombinant SARS-CoV-2 M^{pro}, which is expected given that the SARS-CoV-1 and -CoV-2 M^{pro} share 100% sequence homology across their respective substrate binding sites (*18*). Antiviral activity against SARS-CoV-2 was also observed with PF-00835231 (half-maximal effective concentration (EC_{50}) of 231 nM) by monitoring cytopathic effect (CPE) in epithelial Vero E6 cells. As Vero E6 cells express high levels of the efflux transporter P-glycoprotein, for which **1** is a substrate (*17, 19*), antiviral assays in this cell line were conducted in the presence of the P-glycoprotein efflux inhibitor CP-100356 (*20*). TMPRSS2 expression was not detected in the Vero E6 cells by RTqPCR. The phosphate prodrug form (PF-07304814) of PF-00835231 is currently under investigation as an intravenous treatment option for COVID-19 in hospitalized patients (*20*).

In order to improve upon the low passive absorptive permeability ($P_{app} < 0.207 \times 10^{-6}$ cm/s) (*21*) and poor oral absorption of **1** in animals, we aimed to remove the hydrogen bond donor (HBD) of the P1' α-hydroxymethyl ketone moiety in **1** (Fig. 2A), as increased HBD count has been correlated with poor oral bioavailability (*22*). To this end, we pursued two functional groups precedented as covalent warheads for cysteine proteases in parallel: nitriles (*23, 24*) and benzothiazol-2-yl ketones (*25, 26*). The nitrile compound **2** demonstrated a significant increase in rat oral absorption (oral bioavailability (F) = 7.6% and fraction of oral dose absorbed from the gastrointestinal tract (F_a x F_g) = 38%) (*27*), while maintaining reasonable metabolic stability (intrinsic clearance (CL_{int})) against oxidative metabolism in human liver microsomes (HLM) (*28*) relative to **1** (Fig. 1). However, the in vitro FRET M^{pro} potency (K_i = 27.7 nM) and SARS-CoV-2 antiviral activity (EC_{50} = 1364 nM) of **2** was inferior to **1**. Introduction of a 6,6-dimethyl-3-azabicyclo[3.1.0]hexane as a cyclic leucine mimetic at P2 (Fig. 2B) removed the HBD from the P2/P3 amide linkage. Analog ***3***, resulting from the combination of this cyclic P2 fragment with a P1' benzothiazolyl ketone, displayed high passive absorptive permeability ($P_{app} = 10.3 \times 10^{-6}$ cm/s). The reduced biochemical SARS-CoV-2 M^{pro} inhibitory potency of ***3*** (K_i = 230 nM) relative to other reported benzothiazole-2-yl SARS-CoV-2 M^{pro} inhibitors (*29*) containing leucine P2 groups can be rationalized from the binding mode observed for ***3*** (Fig. 2C). While the 6,6-dimethyl-3-azabicyclo[3.1.0]hexane effectively fills the lipophilic S2 pocket formed by Met49, Met169, His41, and Gln 189, productive hydrogen bonding of the ligand backbone to Gln189 is no longer possible (Fig. 2C). The inferior SARS-CoV-2 M^{pro} potency and the high CL_{int} (337 µl/min/mg) precluded further investments in compound ***3***. Similar to **1**, the P3 indole of ***3*** does not protrude into the S3 pocket (Fig. 2, A and C). To better occupy the S3 pocket, we introduced branched, acyclic P3 groups. The methanesulfonamide in compound **4** extends underneath Gln189, productively engaging P3 pocket residues and achieving improved hydrogen bonding interactions with the Glu166 backbone (Fig. 2D) relative to **1** and ***3***. Compound **4** demonstrated improved SARS-CoV-2 M^{pro} biochemical potency (K_i = 7.93 nM), Vero E6 antiviral activity (EC_{50} = 909 nM), and HLM CL_{int} (127 µl/min/mg) relative to ***3*** (Fig. 1). Examination of the rat pharmacokinetics of **4** also revealed improvements in oral absorption (F = 10%, F_a x F_g = 84%) (Fig. 1). An effort to identify alternate P3 capping groups to sulfonamide led to trifluoroacetamide ***5***. Compound ***5*** exhibited comparable biochemical potency (K_i = 12.1 nM) to **4**, but with greatly improved SARS-CoV-2 Vero E6 antiviral activity (EC_{50} = 85.3 nM) and passive permeability ($P_{app} = 13.1 \times 10^{-6}$ cm/sec) as well as increased metabolic stability in HLM (CL_{int} = 30.3 µl/min/mg) (Fig. 1). ***5*** also shows greatly improved oral pharmacokinetics in both rats (F = 33%, F_a x F_g = 100%) (Fig. 1) and monkeys (F = 7.9%, F_a x F_g = 66%) (table S1). Introduction of the P1' nitrile to this scaffold led to the identification of the clinical candidate PF-07321332 (**6**, Fig. 1). Compound **6** is a potent inhibitor of SARS-CoV-2 M^{pro} biochemical activity (K_i = 3.11 nM) with improved Vero E6 antiviral activity (EC_{50} = 74.5 nM) relative to compounds **2**-**4**. Compound **6** displays a similar binding mode (Fig. 2E) to compound **4**. The P1' nitrile of **6** forms a reversible covalent thioimidate adduct with the catalytic Cys145 (Fig. 2F). Reversibility of M^{pro} inhibition by **6** was demonstrated upon incubation of SARS-CoV-2 M^{pro} (2 mM) with 2 mM of either **6** or an irreversible M^{pro} inhibitor (compound **7**, Fig. 3A) (*17*) for 30 min and monitoring M^{pro} activity following 100-fold dilution of the incubation mixtures. No recovery of activity was observed following M^{pro} incubation with **7**. The recovery of >50% M^{pro} activity following incubation with **6** indicates that inhibition of SARS-CoV-2 M^{pro} is reversible (Fig. 3A). We selected the nitrile compound **6** (named PF-07321332) over compound ***5*** as the clinical candidate based on ease of synthetic scale-up, enhanced solubility that allowed for a simple formulation vehicle in support of pre-clinical toxicology, and reduced propensity for epimerization at the P1 stereocenter.

PF-07321332 demonstrated potent inhibition in FRET M^{pro} assays representing M^{pro} from all coronavirus types known to infect humans (*6, 7, 30*), including beta-

coronaviruses (SARS-CoV-2, SARS-CoV-1, HKU1, OC43, MERS) as well as alpha-coronaviruses (229E, NL63) (Fig. 3B and table S2). No inhibitory effects were noted against several mammalian cysteine (caspase 2, cathepsin B, cathepsin L), serine (chymotrypsin, elastase, thrombin) and aspartyl (cathepsin D) proteases at the highest concentration tested (100 μM) of PF-07321332 (table S3). This was also the case for HIV-1 protease, a viral aspartyl protease (table S3).

The in vitro antiviral activity of PF-07321332 was also evaluated in two physiologically relevant cellular systems; human adenocarcinoma-derived alveolar basal epithelial (A549) cells constitutively expressing ACE2 (*19*) and differentiated normal human bronchial epithelial (dNHBE) cells (*31*). In contrast with Vero E6 cells, A549 and dNHBE cells do not overly express P-glycoprotein, and therefore, co-dosing with a P-glycoprotein inhibitor was not necessary to gauge antiviral activity in these cell lines (*19*). PF-07321332 inhibited SARS-CoV-2 replication as assessed using a nanoluciferase reporter virus in A549-ACE2 cells with EC_{50} and EC_{90} values of 77.9 nM and 215 nM respectively, with no cytotoxicity detected at concentrations up to 3 μM (Fig. 3C and table S4). Treatment of dNHBE cells with varying concentrations of PF-07321332 for 3 days led to inhibition of SARS-CoV-2 viral replication with EC_{50} and EC_{90} values of 61.8 nM and 181 nM, respectively (Fig. 3C) as monitored by titration of virus harvested from the apical compartment using a 50% cell culture infective dose ($CCID_{50}$) assay in Vero76 cells. Increasing the duration of the dNHBE study to 5 days saw viral replication inhibited with EC_{50} and EC_{90} values of 32.6 nM and 56.1 nM (Fig. 3C). Since optimal therapeutic efficacy with marketed viral protease inhibitors and other antiviral agents is generally achieved when the minimum systemic unbound plasma concentrations of inhibitor (C_{min}) are maintained above cellular antiviral EC_{90} (*32*), we selected the more conservative day 3 EC_{90} value of 181 nM PF-07321332 in the dNHBE assay as the C_{min} to be maintained when predicting efficacy in animal models and in the clinic. We further evaluated the in vitro cellular antiviral activity of PF-07321332 against SARS-CoV-1, MERS and human coronavirus 229E using cytopathic effect (CPE) assays. PF-07321332 demonstrated potent antiviral activity against SARS-CoV-1 (EC_{90} = 317 nM), MERS (EC_{90} = 351 nM) and 229E (EC_{90} = 620 nM) in their respective cellular assays (Fig. 3D and table S5).

We evaluated the in vivo antiviral activity of PF-07321332 in a mouse-adapted SARS-CoV-2 (SARS-CoV-2 MA10) model (*33*). Intranasal infection of BALB/c mice with SARS-CoV-2 MA10 leads to ~10% body weight loss and minimal mortality in 10-week-old mice. As shown in Fig. 4A, following infection with SARS-CoV-2 MA10, mice treated twice daily with PF-07321332 (at both 300 mg/kg and 1000 mg/kg doses), were protected from weight loss versus vehicle-treated mice. At 4 days post infection, mice were sacrificed, and lung viral titers were evaluated in $CCID_{50}$ assays. Infected animals in the placebo group (n=12, two independent studies) had robust infection in the lungs (mean lung titer of $\log_{10}$ 4.93 ± 0.140 $CCID_{50}$/ml SARS-CoV-2 MA10) (Fig. 4B) whereas virus levels in mice treated with PF-07321332 were significantly reduced (mean lung titers of $\log_{10}$ 3.53 ± 0.187 and $\log_{10}$ 3.02 ± 0.423 $CCID_{50}$/ml for 300 and 1000 mg/kg PF-07321332-treated groups, respectively). In a satellite group of uninfected mice, the 300 mg/kg BID dose of PF-07321332 used in the mouse-adapted viral in vivo efficacy study maintained C_{min} unbound plasma concentrations above ~0.9 x EC_{90} (Fig. 4C), as defined in the dNHBE primary cell assay. The 1000 mg/kg BID dose of PF-07321332 maintained a C_{min} unbound plasma concentration of ~4 x EC_{90} (Fig. 4C). This confirms that PF-07321332 is effective at reducing SARS-CoV-2 MA10 viral load in mouse lungs at concentrations consistent with the observed in vitro anti-viral potency, and those being targeted clinically.

Disease in this model is manifest by weight loss and pathological changes in the lungs of the infected mice (*33*). Histopathological analysis and immunostaining of lungs from the SARS-CoV-2 MA10 infected mice shows that PF-07321332 limits cellular infiltration (Fig. 4D and fig. S2) and protects lung tissue from damage due to virus replication (Fig. 4E). Immunohistochemical analysis using a viral nucleocapsid antibody to detect viral antigen levels in the lungs revealed that PF-07321332 inhibits virus replication in a dose-dependent manner (Fig. 4E). Lungs from vehicle-treated, infected mice showed the strongest staining whereas mock-infected lungs were negative for nucleocapsid staining. Histopathological evaluation of lungs from the vehicle-treated mice demonstrated evidence of increased perivascular inflammation, bronchial or bronchiolar epithelial degeneration or necrosis, bronchial or bronchiolar inflammation, cellular debris in alveolar lumen, and alveolar inflammation and thickening of the alveolar septum compared to PF-07321332-treated mice and mock-infected mice (fig. S2). Most of the infected mice exhibited multifocal pulmonary lesions, which were significantly reduced in PF-07321332-treated mice.

PF-07321332 exhibited moderate plasma clearance (CL_p) in rats and monkeys, with elimination half-lives ($t_{1/2}$) of 5 hours and <1 hour, respectively, after intravenous dosing (table S6). Following oral administration to rats, crystalline PF-07321332 (10 mg/kg) demonstrated oral dose absorbed (F_a x F_g) and oral availability (F) values ranging from 65-95% and 34-50% respectively, depending on the crystalline form used (Fig. 1 and table S6). Oral administration of PF-07321332 (10 mg/kg) to monkeys led to a relatively poor F of 8.5% (F_a x F_g = 20%) (table S6), which is attributed to first-pass metabolism along the gastrointestinal tract by cytochrome P450 (CYP) enzymes, consistent with rapid ($t_{1/2}$ = 20.5 min, CL_{int} = 33.8 μl/min/mg) NADPH-dependent metabolic turnover of

PF-07321332 in monkey intestinal microsomes (table S7). PF-07321332 was resistant ($t_{1/2}$ > 240 min, CL_{int} <2.89 µl/min/mg) to CYP-mediated metabolism in intestinal microsomes from rat and human. PF-07321332 (0.3–10 µM) exhibited concentration-independent plasma protein binding in rat (mean plasma unbound fraction ($f_{u,p}$) = 0.478), monkey (mean $f_{u,p}$ = 0.434), and human (mean $f_{u,p}$ = 0.310) under equilibrium dialysis conditions (*34*).

Drug-metabolizing enzymes involved in the metabolism of PF-07321332 were also studied. In NADPH-supplemented HLM, PF-07321332 demonstrated moderate CL_{int} (24.5 µl/min/mg) (Fig. 1 and table S7), which was significantly inhibited (≥82%) by the selective CYP3A4/5 inhibitor ketoconazole (*28*) (table S8). Moreover, the oxidative metabolic profile of PF-07321332 in HLM, which includes modifications on the P2 6,6-dimethyl-3-azabicyclo[3.1.0]hexane, the *tert*-butyl group at the P3 position, and the P1 pyrrolidinone ring, was reproduced in incubations of PF-07321332 with recombinant human CYP3A4 (fig. S1). These in vitro studies, which established a predominant role for CYP3A4 in the metabolism of PF-07321332, also presented an opportunity to boost therapeutic concentrations of PF-07321332 in the clinic via co-dosing with the potent CYP3A4 inactivator ritonavir (RTV), which is used as a pharmacokinetic enhancer of several marketed protease inhibitors (e.g., darunavir, lopinavir) that are subject to metabolic clearance via CYP3A4 (*35*, *36*).

PF-07321332 demonstrated a favorable off-target selectivity profile in a broad panel of G protein-coupled receptors, kinases, transporters and phosphodiesterase enzyme inhibitor screens, and was devoid of activity against the cardiac ion channels $K_v1.1$, $Ca_v1.2$, and $Na_v1.5$ (tables S9 and S10). PF-07321332 was not mutagenic or clastogenic in in vitro genetic toxicity studies and was negative in an in vivo rat micronucleus assay (table S11). Repeat oral dosing of PF-07321332 in 2-week regulatory toxicity studies in monkeys (60-600 mg/kg) and rats (40-1000mg/kg) led to dose-dependent increases in both maximal plasma concentrations (C_{max}) and area-under-the-plasma concentration versus time curves (AUC) (Fig. 5, A and B, and table S12). This resulted in unbound C_{max} and average concentrations (C_{av}) margins of 273-fold and 65-fold in rats (day 14, 1000 mg/kg) and 510-fold and 245-fold in monkeys (day 15, 600 mg/kg) over the measured unbound EC_{90} value of PF-07321332 determined in the SARS-CoV-2 day three dNHBE cellular assay. PF-07321332 was well tolerated with no adverse findings in either species; the corresponding no observed adverse effect levels (NOAEL) were the highest doses tested (600 mg/kg/day in monkeys and 1000 mg/kg/day in rats).

The safety, tolerability, and pharmacokinetics of PF-07321332 as a single agent and in combination with RTV are under investigation in a randomized, double-blind, placebo-controlled, single ascending dose study in healthy adult participants (table S13, ClinicalTrials.gov Identifier: NCT04756531). At each dose tested, 4 participants were randomized to receive active treatment while 2 participants received placebo. In the PF-07321332/RTV co-administration dosing paradigm, each subject (active and placebo) received one tablet (100 mg) of RTV at -12 hours, 0 hours and 12 hours. PF-07321332 was administered as an oral suspension under fasted conditions at 0 hours (minimum fast of ~10 hours prior to treatment). Preliminary plasma concentration versus time pharmacokinetic profiles achieved from two oral doses, PF-07321332 (150 mg) alone and PF-07321332 (250 mg) with RTV are presented in Fig. 5C. PF-07321332 was safe and well tolerated, and exhibited a significant boost in plasma concentrations when co-administered with RTV. Oral plasma concentrations of PF-07321332 (250 mg with RTV) were considerably above the SARS-COV-2 antiviral EC_{90} value (total EC_{90} = 292 ng/ml, unbound EC_{90} = 90.5 ng/ml, 181 nM) at 12 hours post-dose, thus increasing confidence in achieving robust pan-coronavirus anti-viral activity clinically (Fig. 5D). Based on these observations and the high safety margins at the NOAEL doses in animals, the efficacy of PF-07321332 in COVID-19 patients will be assessed with a twice daily dosing paradigm with the potential to increase the dose of PF-07321332 as a single agent and/or co-administration with RTV.

REFERENCES AND NOTES

1. V. M. Corman, D. Muth, D. Niemeyer, C. Drosten, Hosts and sources of endemic human coronaviruses. *Adv. Virus Res.* **100**, 163–188 (2018). doi:10.1016/bs.aivir.2018.01.001 Medline
2. WHO Solidarity Trial Consortium, Repurposed antiviral drugs for Covid-19 - Interim WHO Solidarity Trial results. *N. Engl. J. Med.* **384**, 497–511 (2021). doi:10.1056/NEJMoa2023184 Medline
3. L. Riva, S. Yuan, X. Yin, L. Martin-Sancho, N. Matsunaga, L. Pache, S. Burgstaller-Muehlbacher, P. D. De Jesus, P. Teriete, M. V. Hull, M. W. Chang, J. F. Chan, J. Cao, V. K. Poon, K. M. Herbert, K. Cheng, T. H. Nguyen, A. Rubanov, Y. Pu, C. Nguyen, A. Choi, R. Rathnasinghe, M. Schotsaert, L. Miorin, M. Dejosez, T. P. Zwaka, K. Y. Sit, L. Martinez-Sobrido, W. C. Liu, K. M. White, M. E. Chapman, E. K. Lendy, R. J. Glynne, R. Albrecht, E. Ruppin, A. D. Mesecar, J. R. Johnson, C. Benner, R. Sun, P. G. Schultz, A. I. Su, A. García-Sastre, A. K. Chatterjee, K. Y. Yuen, S. K. Chanda, Discovery of SARS-CoV-2 antiviral drugs through large-scale compound repurposing. *Nature* **586**, 113–119 (2020). doi:10.1038/s41586-020-2577-1 Medline
4. A. Wahl, L. E. Gralinski, C. E. Johnson, W. Yao, M. Kovarova, K. H. Dinnon 3rd, H. Liu, V. J. Madden, H. M. Krzystek, C. De, K. K. White, K. Gully, A. Schäfer, T. Zaman, S. R. Leist, P. O. Grant, G. R. Bluemling, A. A. Kolykhalov, M. G. Natchus, F. B. Askin, G. Painter, E. P. Browne, C. D. Jones, R. J. Pickles, R. S. Baric, J. V. Garcia, SARS-CoV-2 infection is effectively treated and prevented by EIDD-2801. *Nature* **591**, 451–457 (2021). doi:10.1038/s41586-021-03312-w Medline
5. S. S. Good, J. Westover, K. H. Jung, X. J. Zhou, A. Moussa, P. La Colla, G. Collu, B. Canard, J. P. Sommadossi, AT-527, a double prodrug of a guanosine nucleotide analog, is a potent inhibitor of SARS-CoV-2 in vitro and a promising oral antiviral for treatment of COVID-19. *Antimicrob. Agents Chemother.* **65**, e02479–e02420 (2021). doi:10.1128/AAC.02479-20 Medline
6. F. Wu, S. Zhao, B. Yu, Y. M. Chen, W. Wang, Z. G. Song, Y. Hu, Z. W. Tao, J. H. Tian, Y. Y. Pei, M. L. Yuan, Y. L. Zhang, F. H. Dai, Y. Liu, Q. M. Wang, J. J. Zheng, L. Xu, E. C. Holmes, Y. Z. Zhang, A new coronavirus associated with human respiratory disease in China. *Nature* **579**, 265–269 (2020). doi:10.1038/s41586-020-2008-3 Medline

7. P. Zhou, X. L. Yang, X. G. Wang, B. Hu, L. Zhang, W. Zhang, H. R. Si, Y. Zhu, B. Li, C. L. Huang, H. D. Chen, J. Chen, Y. Luo, H. Guo, R. D. Jiang, M. Q. Liu, Y. Chen, X. R. Shen, X. Wang, X. S. Zheng, K. Zhao, Q. J. Chen, F. Deng, L. L. Liu, B. Yan, F. X. Zhan, Y. Y. Wang, G. F. Xiao, Z. L. Shi, A pneumonia outbreak associated with a new coronavirus of probable bat origin. *Nature* **579**, 270–273 (2020). doi:10.1038/s41586-020-2012-7 Medline
8. T. Pillaiyar, M. Manickam, V. Namasivayam, Y. Hayashi, S. H. Jung, An overview of Severe Acute Respiratory Syndrome-Coronavirus (SARS-CoV) 3CL protease inhibitors: Peptidomimetics and small molecule chemotherapy. *J. Med. Chem.* **59**, 6595–6628 (2016). doi:10.1021/acs.jmedchem.5b01461 Medline
9. Z. Jin, X. Du, Y. Xu, Y. Deng, M. Liu, Y. Zhao, B. Zhang, X. Li, L. Zhang, C. Peng, Y. Duan, J. Yu, L. Wang, K. Yang, F. Liu, R. Jiang, X. Yang, T. You, X. Liu, X. Yang, F. Bai, H. Liu, X. Liu, L. W. Guddat, W. Xu, G. Xiao, C. Qin, Z. Shi, H. Jiang, Z. Rao, H. Yang, Structure of M^{pro} from SARS-CoV-2 and discovery of its inhibitors. *Nature* **582**, 289–293 (2020). doi:10.1038/s41586-020-2223-y Medline
10. I. Schechter, A. Berger, On the size of the active site in proteases. I. Papain. *Biochem. Biophys. Res. Commun.* **27**, 157–162 (1967). doi:10.1016/S0006-291X(67)80055-X Medline
11. W. Rut, K. Groborz, L. Zhang, X. Sun, M. Zmudzinski, B. Pawlik, X. Wang, D. Jochmans, J. Neyts, W. Młynarski, R. Hilgenfeld, M. Drag, SARS-CoV-2 M^{pro} inhibitors and activity-based probes for patient-sample imaging. *Nat. Chem. Biol.* **17**, 222–228 (2021). doi:10.1038/s41589-020-00689-z Medline
12. K. Anand, J. Ziebuhr, P. Wadhwani, J. R. Mesters, R. Hilgenfeld, Coronavirus main proteinase (3CLpro) structure: Basis for design of anti-SARS drugs. *Science* **300**, 1763–1767 (2003). doi:10.1126/science.1085658 Medline
13. L. Zhang, D. Lin, Y. Kusov, Y. Nian, Q. Ma, J. Wang, A. von Brunn, P. Leyssen, K. Lanko, J. Neyts, A. de Wilde, E. J. Snijder, H. Liu, R. Hilgenfeld, α-Ketoamides as broad-spectrum inhibitors of coronavirus and enterovirus replication: Structure-based design, synthesis, and activity assessment. *J. Med. Chem.* **63**, 4562–4578 (2020). doi:10.1021/acs.jmedchem.9b01828 Medline
14. A. K. Ghosh, H. L. Osswald, G. Prato, Recent progress in the development of HIV-1 protease inhibitors for the treatment of HIV/AIDS. *J. Med. Chem.* **59**, 5172–5208 (2016). doi:10.1021/acs.jmedchem.5b01697 Medline
15. R. Cannalire, M. L. Barreca, G. Manfroni, V. Cecchetti, A journey around the medicinal chemistry of Hepatitis C virus inhibitors targeting NS4B: From target to preclinical drug candidates. *J. Med. Chem.* **59**, 16–41 (2016). doi:10.1021/acs.jmedchem.5b00825 Medline
16. J. Qiao, Y.-S. Li, R. Zeng, F.-L. Liu, R.-H. Luo, C. Huang, Y.-F. Wang, J. Zhang, B. Quan, C. Shen, X. Mao, X. Liu, W. Sun, W. Yang, X. Ni, K. Wang, L. Xu, Z.-L. Duan, Q.-C. Zou, H.-L. Zhang, W. Qu, Y.-H.-P. Long, M.-H. Li, R.-C. Yang, X. Liu, J. You, Y. Zhou, R. Yao, W.-P. Li, J.-M. Liu, P. Chen, Y. Liu, G.-F. Lin, X. Yang, J. Zou, L. Li, Y. Hu, G.-W. Lu, W.-M. Li, Y.-Q. Wei, Y.-T. Zheng, J. Lei, S. Yang, SARS-CoV-2 M^{pro} inhibitors with antiviral activity in a transgenic mouse model. *Science* **371**, 1374–1378 (2021). doi:10.1126/science.abf1611 Medline
17. R. L. Hoffman, R. S. Kania, M. A. Brothers, J. F. Davies, R. A. Ferre, K. S. Gajiwala, M. He, R. J. Hogan, K. Kozminski, L. Y. Li, J. W. Lockner, J. Lou, M. T. Marra, L. J. Mitchell Jr., B. W. Murray, J. A. Nieman, S. Noell, S. P. Planken, T. Rowe, K. Ryan, G. J. Smith 3rd, J. E. Solowiej, C. M. Steppan, B. Taggart, Discovery of ketone-based covalent inhibitors of coronavirus 3CL proteases for the potential therapeutic treatment of COVID-19. *J. Med. Chem.* **63**, 12725–12747 (2020). doi:10.1021/acs.jmedchem.0c01063 Medline
18. L. Zhang, D. Lin, X. Sun, U. Curth, C. Drosten, L. Sauerhering, S. Becker, K. Rox, R. Hilgenfeld, Crystal structure of SARS-CoV-2 main protease provides a basis for design of improved α-ketoamide inhibitors. *Science* **368**, 409–412 (2020). doi:10.1126/science.abb3405 Medline
19. M. de Vries, A. S. Mohamed, R. A. Prescott, A. M. Valero-Jimenez, L. Desvignes, R. O'Connor, C. Steppan, J. C. Devlin, E. Ivanova, A. Herrera, A. Schinlever, P. Loose, K. Ruggles, S. B. Koralov, A. S. Anderson, J. Binder, M. Dittmann, A comparative analysis of SARS-CoV-2 antivirals characterizes $3CL^{pro}$ inhibitor PF-00835231 as a potential new treatment for COVID-19. *J. Virol.* **95**, e01819–e01820 (2021). doi:10.1128/JVI.01819-20 Medline
20. B. Boras, R. M. Jones, B. J. Anson, D. Arenson, L. Aschenbrenner, M. A. Bakowski, N. Beutler, J. Binder, E. Chen, H. Eng, J. Hammond, R. Hoffman, E. P. Kadar, R. Kania, E. Kimoto, M. G. Kirkpatrick, L. Lanyon, E. K. Lendy, J. R. Lillis, S. A. Luthra, C. Ma, S. Noell, R. S. Obach, M. N. O' Brien, R. O'Connor, K. Ogilvie, D. Owen, M. Pettersson, M. R. Reese, T. F. Rogers, M. I. Rossulek, J. G. Sathish, C. Steppan, M. Ticehurst, L. W. Updyke, Y. Zhu, J. Wang, A. K. Chatterjee, A. D. Mesecar, A. S. Anderson, C. Allerton, Discovery of a novel inhibitor of coronavirus 3CL protease as a clinical candidate for the potential treatment of COVID-19. bioRxiv 293498 [Preprint] (2020). https://www.biorxiv.org/content/10.1101/2020.09.12.293498v2.
21. L. Di, C. Whitney-Pickett, J. P. Umland, H. Zhang, X. Zhang, D. F. Gebhard, Y. Lai, J. J. Federico 3rd, R. E. Davidson, R. Smith, E. L. Reyner, C. Lee, B. Feng, C. Rotter, M. V. Varma, S. Kempshall, K. Fenner, A. F. El-Kattan, T. E. Liston, M. D. Troutman, Development of a new permeability assay using low-efflux MDCKII cells. *J. Pharm. Sci.* **100**, 4974–4985 (2011). doi:10.1002/jps.22674 Medline
22. D. F. Veber, S. R. Johnson, H. Y. Cheng, B. R. Smith, K. W. Ward, K. D. Kopple, Molecular properties that influence the oral bioavailability of drug candidates. *J. Med. Chem.* **45**, 2615–2623 (2002). doi:10.1021/jm020017n Medline
23. J. B. Moon, R. S. Coleman, R. P. Hanzlik, Reversible covalent inhibition of papain by a peptide nitrile. Carbon-13 NMR evidence for a thioimidate ester adduct. *J. Am. Chem. Soc.* **108**, 1350–1351 (2002). doi:10.1021/ja00266a066
24. C.-P. Chuck, C. Chen, Z. Ke, D. Chi-Cheong Wan, H.-F. Chow, K.-B. Wong, Design, synthesis and crystallographic analysis of nitrile-based broad-spectrum peptidomimetic inhibitors for coronavirus 3C-like proteases. *Eur. J. Med. Chem.* **59**, 1–6 (2013). doi:10.1016/j.ejmech.2012.10.053 Medline
25. S. Konno, P. Thanigaimalai, T. Yamamoto, K. Nakada, R. Kakiuchi, K. Takayama, Y. Yamazaki, F. Yakushiji, K. Akaji, Y. Kiso, Y. Kawasaki, S. E. Chen, E. Freire, Y. Hayashi, Design and synthesis of new tripeptide-type SARS-CoV 3CL protease inhibitors containing an electrophilic arylketone moiety. *Bioorg. Med. Chem.* **21**, 412–424 (2013). doi:10.1016/j.bmc.2012.11.017 Medline
26. P. S. Dragovich, R. Zhou, S. E. Webber, T. J. Prins, A. K. Kwok, K. Okano, S. A. Fuhrman, L. S. Zalman, F. C. Maldonado, E. L. Brown, J. W. Meador 3rd, A. K. Patick, C. E. Ford, M. A. Brothers, S. L. Binford, D. A. Matthews, R. A. Ferre, S. T. Worland, Structure-based design of ketone-containing, tripeptidyl human rhinovirus 3C protease inhibitors. *Bioorg. Med. Chem. Lett.* **10**, 45–48 (2000). doi:10.1016/S0960-894X(99)00587-9 Medline
27. M. Kato, K. Chiba, A. Hisaka, M. Ishigami, M. Kayama, N. Mizuno, Y. Nagata, S. Takakuwa, Y. Tsukamoto, K. Ueda, H. Kusuhara, K. Ito, Y. Sugiyama, The intestinal first-pass metabolism of substrates of CYP3A4 and P-glycoprotein-quantitative analysis based on information from the literature. *Drug Metab. Pharmacokinet.* **18**, 365–372 (2003). doi:10.2133/dmpk.18.365 Medline
28. R. L. Walsky, R. S. Obach, Validated assays for human cytochrome P450 activities. *Drug Metab. Dispos.* **32**, 647–660 (2004). doi:10.1124/dmd.32.6.647 Medline
29. S. I. Hattori, N. Higashi-Kuwata, H. Hayashi, S. R. Allu, J. Raghavaiah, H. Bulut, D. Das, B. J. Anson, E. K. Lendy, Y. Takamatsu, N. Takamune, N. Kishimoto, K. Murayama, K. Hasegawa, M. Li, D. A. Davis, E. N. Kodama, R. Yarchoan, A. Wlodawer, S. Misumi, A. D. Mesecar, A. K. Ghosh, H. Mitsuya, A small molecule compound with an indole moiety inhibits the main protease of SARS-CoV-2 and blocks virus replication. *Nat. Commun.* **12**, 668 (2021). doi:10.1038/s41467-021-20900-6 Medline
30. J. Cui, F. Li, Z. L. Shi, Origin and evolution of pathogenic coronaviruses. *Nat. Rev. Microbiol.* **17**, 181–192 (2019). doi:10.1038/s41579-018-0118-9 Medline
31. A. Barilli, R. Visigalli, F. Ferrari, M. Di Lascia, B. Riccardi, P. Puccini, V. Dall'Asta, B. M. Rotoli, Organic cation transporters (OCTs) in EpiAirway™, a cellular model of normal human bronchial epithelium. *Biomedicines* **8**, 127 (2020). doi:10.3390/biomedicines8050127 Medline
32. M. B. Reddy, P. N. Morcos, S. Le Pogam, Y. Ou, K. Frank, T. Lave, P. Smith, Pharmacokinetic/Pharmacodynamic predictors of clinical potency for hepatitis C virus nonnucleoside polymerase and protease inhibitors. *Antimicrob. Agents Chemother.* **56**, 3144–3156 (2012). doi:10.1128/AAC.06283-11 Medline
33. S. R. Leist, K. H. Dinnon 3rd, A. Schäfer, L. V. Tse, K. Okuda, Y. J. Hou, A. West, C. E. Edwards, W. Sanders, E. J. Fritch, K. L. Gully, T. Scobey, A. J. Brown, T. P. Sheahan, N. J. Moorman, R. C. Boucher, L. E. Gralinski, S. A. Montgomery, R. S. Baric, A mouse-adapted SARS-CoV-2 induces acute lung injury and mortality in standard laboratory mice. *Cell* **183**, 1070–1085.e12 (2020). doi:10.1016/j.cell.2020.09.050 Medline
34. M. J. Banker, T. H. Clark, J. A. Williams, Development and validation of a 96-well equilibrium dialysis apparatus for measuring plasma protein binding. *J. Pharm. Sci.* **92**, 967–974 (2003). doi:10.1002/jps.10332 Medline

35. K. McKeage, C. M. Perry, S. J. Keam, Darunavir: A review of its use in the management of HIV infection in adults. *Drugs* **69**, 477–503 (2009). doi:10.2165/00003495-200969040-00007 Medline
36. R. S. Cvetkovic, K. L. Goa, Lopinavir/ritonavir: A review of its use in the management of HIV infection. *Drugs* **63**, 769–802 (2003). doi:10.2165/00003495-200363080-00004 Medline
37. A. M. Prior, Y. Kim, S. Weerasekara, M. Moroze, K. R. Alliston, R. A. Uy, W. C. Groutas, K. O. Chang, D. H. Hua, Design, synthesis, and bioevaluation of viral 3C and 3C-like protease inhibitors. *Bioorg. Med. Chem. Lett.* **23**, 6317–6320 (2013). doi:10.1016/j.bmcl.2013.09.070 Medline
38. P. Thanigaimalai, S. Konno, T. Yamamoto, Y. Koiwai, A. Taguchi, K. Takayama, F. Yakushiji, K. Akaji, S. E. Chen, A. Naser-Tavakolian, A. Schön, E. Freire, Y. Hayashi, Development of potent dipeptide-type SARS-CoV 3CL protease inhibitors with novel P3 scaffolds: Design, synthesis, biological evaluation, and docking studies. *Eur. J. Med. Chem.* **68**, 372–384 (2013). doi:10.1016/j.ejmech.2013.07.037 Medline
39. Use of the IMCA-CAT beamline 17-ID (or 17-BM) at the Advanced Photon Source was supported by the companies of the Industrial Macromolecular Crystallography Association through a contract with Hauptman-Woodward Medical Research Institute.
40. This research used resources at the Industrial Macromolecular Crystallography Association Collaborative Access Team (IMCA-CAT) beamline 17-ID, supported by the companies of the Industrial Macromolecular Crystallography Association through a contract with Hauptman-Woodward Medical Research Institute.
41. This research used resources of the Advanced Photon Source, a U.S. Department of Energy (DOE) Office of Science User Facility operated for the DOE Office of Science by Argonne National Laboratory under Contract No. DE-AC02-06CH11357.
42. C. Vonrhein, C. Flensburg, P. Keller, A. Sharff, O. Smart, W. Paciorek, T. Womack, G. Bricogne, Data processing and analysis with the autoPROC toolbox. *Acta Crystallogr. D Biol. Crystallogr.* **67**, 293–302 (2011). doi:10.1107/S0907444911007773 Medline
43. I. J. Tickle, F. C. P. Keller, W. Paciorek, A. Sharff, C. Vonrhein, G. Bricogne, "STARANISO" (Global Phasing Ltd., 2018).
44. G. Bricogne, E. Blanc, M. Brandl, C. Flensburg, P. Keller, W. Paciorek, P. Roversi, A. Sharff, O. S. Smart, C. Vonrhein, T. O. Womack, "BUSTER version 2.11.4" (Global Phasing Ltd., 2016).
45. A. J. McCoy, R. W. Grosse-Kunstleve, P. D. Adams, M. D. Winn, L. C. Storoni, R. J. Read, *Phaser* crystallographic software. *J. Appl. Cryst.* **40**, 658–674 (2007). doi:10.1107/S0021889807021206 Medline
46. A. Vagin, A. Teplyakov, Molecular replacement with MOLREP. *Acta Crystallogr.* **66**, 22–25 (2010). doi:10.1107/S0907444909042589 Medline
47. M. D. Winn, C. C. Ballard, K. D. Cowtan, E. J. Dodson, P. Emsley, P. R. Evans, R. M. Keegan, E. B. Krissinel, A. G. Leslie, A. McCoy, S. J. McNicholas, G. N. Murshudov, N. S. Pannu, E. A. Potterton, H. R. Powell, R. J. Read, A. Vagin, K. S. Wilson, Overview of the CCP4 suite and current developments. *Acta Crystallogr. D Biol. Crystallogr.* **67**, 235–242 (2011). doi:10.1107/S0907444910045749 Medline
48. OpenEye Scientific, "AFITT 2.4.1.2: OpenEye Scientific Software" (OpenEye Scientific, 2021); https://www.eyesopen.com/afitt.
49. S. Wlodek, A. G. Skillman, A. Nicholls, Automated ligand placement and refinement with a combined force field and shape potential. *Acta Crystallogr. D Biol. Crystallogr.* **62**, 741–749 (2006). doi:10.1107/S0907444906016076 Medline
50. P. Emsley, B. Lohkamp, W. G. Scott, K. Cowtan, Features and development of Coot. *Acta Crystallogr. D Biol. Crystallogr.* **66**, 486–501 (2010). doi:10.1107/S0907444910007493 Medline
51. M. S. Weiss, R. Hilgenfeld, On the use of the merging R factor as a quality indicator for X-ray data. *J. Appl. Cryst.* **30**, 203–205 (1997). doi:10.1107/S0021889897003907
52. P. A. Karplus, K. Diederichs, Linking crystallographic model and data quality. *Science* **336**, 1030–1033 (2012). doi:10.1126/science.1218231 Medline
53. A. T. Brünger, Free R value: Cross-validation in crystallography. *Methods Enzymol.* **277**, 366–396 (1997). doi:10.1016/S0076-6879(97)77021-6 Medline
54. V. Grum-Tokars, K. Ratia, A. Begaye, S. C. Baker, A. D. Mesecar, Evaluating the 3C-like protease activity of SARS-Coronavirus: Recommendations for standardized assays for drug discovery. *Virus Res.* **133**, 63–73 (2008). doi:10.1016/j.virusres.2007.02.015 Medline
55. Y. Kim, S. Lovell, K. C. Tiew, S. R. Mandadapu, K. R. Alliston, K. P. Battaile, W. C. Groutas, K. O. Chang, Broad-spectrum antivirals against 3C or 3C-like proteases of picornaviruses, noroviruses, and coronaviruses. *J. Virol.* **86**, 11754–11762 (2012). doi:10.1128/JVI.01348-12 Medline
56. L. J. Reed, H. Muench, A simple method of estimating fifty percent endpoints. *Am. J. Epidemiol.* **27**, 493–497 (1938). doi:10.1093/oxfordjournals.aje.a118408
57. R. S. Obach, J. G. Baxter, T. E. Liston, B. M. Silber, B. C. Jones, F. MacIntyre, D. J. Rance, P. Wastall, The prediction of human pharmacokinetic parameters from preclinical and in vitro metabolism data. *J. Pharmacol. Exp. Ther.* **283**, 46–58 (1997) doi. Medline
58. B. Davies, T. Morris, Physiological parameters in laboratory animals and humans. *Pharm. Res.* **10**, 1093–1095 (1993). doi:10.1023/A:1018943613122 Medline
59. S. Hamada, S. Sutou, T. Morita, A. Wakata, S. Asanami, S. Hosoya, S. Ozawa, K. Kondo, M. Nakajima, H. Shimada, K. Osawa, Y. Kondo, N. Asano, S. Sato, H. Tamura, N. Yajima, R. Marshall, C. Moore, D. H. Blakey, L. M. Schechtman, J. L. Weaver, D. K. Torous, R. Proudlock, S. Ito, C. Namiki, M. Hayashi, Evaluation of the rodent micronucleus assay by a 28-day treatment protocol: Summary of the 13th Collaborative Study by the Collaborative Study Group for the Micronucleus Test (CSGMT)/Environmental Mutagen Society of Japan (JEMS)-Mammalian Mutagenicity Study Group (MMS). *Environ. Mol. Mutagen.* **37**, 93–110 (2001). doi:10.1002/em.1017 Medline
60. M. Hayashi, J. T. MacGregor, D. G. Gatehouse, I.-D. Adler, D. H. Blakey, S. D. Dertinger, G. Krishna, T. Morita, A. Russo, S. Sutou, In vivo rodent erythrocyte micronucleus assay. II. Some aspects of protocol design including repeated treatments, integration with toxicity testing, and automated scoring. *Environ. Mol. Mutagen.* **35**, 234–252 (2000). doi:10.1002/(SICI)1098-2280(2000)35:3<234:AID-EM10>3.0.CO;2-L Medline
61. Organisation for Economic Co-operation and Development, "Test no. 474: Mammalian erythrocyte micronucleus test (OECD, 2016); https://www.oecd.org/env/test-no-474-mammalian-erythrocyte-micronucleus-test-9789264264762-en.htm.
62. International Council for Harmonisation of Technical Requirements for Pharmaceuticals for Human Use, "Guidance on genotoxicity testing and data interpretation for pharmaceuticals intended for human use" (ICH, 2011); https://database.ich.org/sites/default/files/S2%28R1%29%20Guideline.pdf.
63. S. D. Dertinger, D. K. Torous, K. R. Tometsko, Simple and reliable enumeration of micronucleated reticulocytes with a single-laser flow cytometer. *Mutat. Res.* **371**, 283–292 (1996). doi:10.1016/S0165-1218(96)90117-2 Medline
64. M. H. L. Green, W. J. Muriel, Mutagen testing using TRP+ reversion in Escherichia coli. *Mutat. Res.* **38**, 3–32 (1976). doi:10.1016/0165-1161(76)90076-5 Medline
65. D. M. Maron, B. N. Ames, Revised methods for the Salmonella mutagenicity test. *Mutat. Res.* **113**, 173–215 (1983). doi:10.1016/0165-1161(83)90010-9 Medline
66. Organisation for Economic Co-operation and Development, "Test no. 471: Bacterial reverse mutation test" (OECD, 2020); https://www.oecd-ilibrary.org/environment/test-no-471-bacterial-reverse-mutation-test_9789264071247-en.
67. M. Kirsch-Volders, T. Sofuni, M. Aardema, S. Albertini, D. Eastmond, M. Fenech, M. Ishidate Jr., E. Lorge, H. Norppa, J. Surrallés, W. von der Hude, A. Wakata, Report from the In Vitro Micronucleus Assay Working Group. *Environ. Mol. Mutagen.* **35**, 167–172 (2000). doi:10.1002/(SICI)1098-2280(2000)35:3<167:AID-EM3>3.0.CO;2-G Medline
68. J. M. Parry, A. Sors, The detection and assessment of the aneugenic potential of environmental chemicals: The European Community Aneuploidy Project. *Mutat. Res.* **287**, 3–15 (1993). doi:10.1016/0027-5107(93)90140-B Medline
69. Organisation for Economic Co-operation and Development, "Test no. 487: In vitro mammalian cell micronucleus test" (OECD, 2016); https://www.oecd.org/chemicalsafety/test-no-487-in-vitro-mammalian-cell-micronucleus-test-9789264264861-en.htm.
70. Y. Cheng, W. H. Prusoff, Relationship between the inhibition constant (K1) and the concentration of inhibitor which causes 50 per cent inhibition (I50) of an enzymatic reaction. *Biochem. Pharmacol.* **22**, 3099–3108 (1973). doi:10.1016/0006-2952(73)90196-2 Medline

ACKNOWLEDGMENTS

The authors would like to thank the participants of the FIH study. We would also like to acknowledge the significant number of Pfizer colleagues who have contributed to the COVID-19 oral protease program across a number of disciplines. In particular, we acknowledge Sylvie Sakata, Joel Arcari, Jinzhi Zhang for external research resourcing, Kathleen Farley for NMR studies, Lorraine Lanyon for protease panel data, Yajing Lian, Erik LaChapelle, Stephen Wright, Steven O'Neil, Eddie Yang, John Humphrey, Brian Boscoe for compound synthesis, Steve Jenkinson for safety pharmacology data, Kevin Ryan for structural biology support, Elizabeth Collins, Chris Allais for FIH-enabling active pharmaceutical ingredient supply, Fran Clark for bioanalysis, Haihong Shi for clinical assay support, Gianluca Nucci, Art Bergman for first-in-human study design and clinical pharmacology, Frances Hackman for clinical statistics, Sima Toussi for medical monitoring, Karen Bartsch for clinical study leadership, Sylvester Pawlak for clinical trial leadership, Claudine Fredette for clinical trial project management, Ding Ding for regulatory documentation support, and Mikael Dolsten for scientific discussion and advice. This research used resources of the Advanced Photon Source, a U.S. Department of Energy (DOE) Office of Science User Facility, operated for the DOE Office of Science by Argonne National Laboratory under Contract No. DE-AC02-06CH11357. Extraordinary facility operations were supported in part by the DOE Office of Science through the National Virtual Biotechnology Laboratory, a consortium of DOE national laboratories focused on the response to COVID-19, with funding provided by the Coronavirus CARES Act. **Funding:** This study was sponsored by Pfizer, Inc. Author contributions: Conceptualization: CMNA, ASA, DRO, MP Formal Analysis: LD, BB, SEG, QY, DKR, JJN, AD, RSO, RSPS Investigation: MA, SB, JCL, JL, KO, LW, RF, KSG, WL, RSO, DKR, SAG, LA, SN, HE Methodology: JBT, QY, MFS, PRV, MRR, MP, DRO, NCP, AC, EPK, KJC, RSPS Project Administration: DRO, MRR, JBT, ASK, CMS, LU, JGS, BLH, YZ, SWM, RDC, NCP Resources: AD, JJN, KJC Supervision: MRR, CES, AES, BLH, PRV, RDC Visualization: SWM, DKR, SN, BB, LA, HE Writing – original draft: DRO, ASK, MFS, CMS, RDC, MRR, JGS, CMS, YZ Writing – review and editing: DRO, ASK, MFS, ASA, CMNA **Competing interests:** DRO, CMNA, ASA, LA, MA, SB, BB, RDC, AC, KJC, AD, LD, HE, RF, KSG, SEG, EPK, ASK, JCL, JL, WL, SN, RSO, KO, NCP, DKR, MRR, MFS, JGS, RPS, CMS, AS, JBT, LU, PRV, LW, QY, YZ are employees of Pfizer and some of the authors are shareholders in Pfizer Inc. SWM, JJN, MP were employees of Pfizer Inc. during part of this study. **Data and materials availability:** All non-clinical data are available in the main text or the supplementary materials. X-ray coordinates and structure factors are deposited at the RCSB Protein Data Bank under accession codes 7RFR, 7RFU, 7RFS and 7RFW. Individualized Fig. 5 data, and statistical analysis plan are available on www.Figshare.com with the following DOI: 10.25454/pfizer.figshare.16699669. Pfizer compound use requests are processed via the 'Pure Compound Grants' program see https://www.cybergrants.com/pfizer/Research. Pfizer Inc. has applied for patent applications covering PF-07321332 as well as related compounds. A phase 1 clinical trial has been registered at clinicaltrials.gov (identifier NCT04756531).

SUPPLEMENTARY MATERIALS

science.org/doi/10.1126/science.abl4784
Materials and Methods
Figs. S1 and S2
Tables S1 to S13
References (*37*–*70*)
MDAR Reproducibility Checklist

15 July 2021; accepted 28 October 2021
Published online 2 November 2021
10.1126/science.abl4784

Number/Structure	SARS-CoV2 M^{pro} K_i (nM)[a]	VeroE6-enACE2 CPE EC_{50} (nM)[b]	MDCK-LE P_{app} (x 10^{-6} cm/sec)[c]	HLM CL_{int} (µl/min/mg)[d]	Rat CL_p (mL/min/kg)[e]	Oral F (%)[e,f]	F_a x F_g (%)[e,h]
1 (PF-00835231) 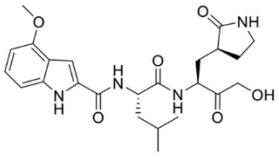	0.271 (0.155 – 0.471, n=6)	231 (158 – 338, n=8)	< 0.207 ± 0.048 (n=6)	7.47 ± 0.88	27.0 ± 3.1	1.4 ± 0.8	3.3
2 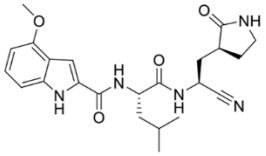	27.7 (18.4 – 41.7, n=5)	1364 (860 – 2164, n=15)	0.945 ± 0.281 (n=6)	34.4 ± 0.7	39.3 (37.0, 41.5)	7.6 (7.4, 7.8)	38
3 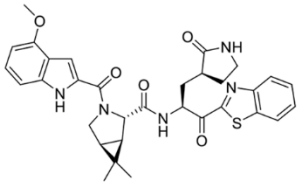	230 (181 – 292, n=4)	5593 (3457 – 9051, n=8)	10.3 ± 2.4 (n=6)	337 ± 9	N.D.	N.D.	N.D.
4 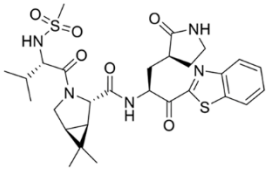	7.93 (3.62 – 17.4, n=5)	909 (557 – 1482, n=14)	1.56 ± 0.38 (n=6)	127 ± 3	42.9 (38.2, 47.6)	10 (7.5, 13)	84
5 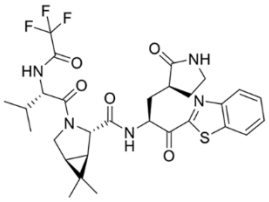	12.1 (8.05 – 18.1, n=7)	85.3 (76.5– 95.2, n=36)	13.1 ± 2.0 (n=8)	30.3 ± 0.6	31.0 (30.6, 31.4)	33 (33, 34)	100
6 (PF-07321332) 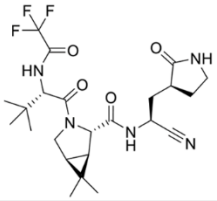	3.11 (1.47 – 6.59, n=6)	74.5 (66.5 – 83.4, n=20)	1.71 ± 0.28 (n=4)	24.5 ± 0.2	27.2 (22.5, 31.9)	50 (30, 71), 34 ±19[g]	95, 65[g]

Fig. 1. In vitro and in vivo parameters optimized in identifying oral SARS-CoV-2 M^{pro} inhibitors. [a]K_i values were fit to the Morrison equation with substrate, K_m and M^{pro} concentration parameters fixed to values described in the supplemental information. Data are geometric mean values with 95% confidence interval (CI) values and replicate numbers in parentheses. [b]EC_{50} values were calculated using data normalized to controls within the assay and fit to a 4-parameter logistic curve fit (see supplemental information for details). Data are geometric mean values with 95% CI values and replicate numbers in parentheses. [c]Apparent passive permeability (P_{app}) from apical to basolateral direction was determined in Madin-Darby canine kidney-low efflux (MDCK-LE) cells (*21*). [d]CL_{int} refers to total intrinsic clearance obtained from scaling of half-lives of test compounds in NADPH-supplemented HLM (*28*). Incubations were conducted on a single day in triplicate. [e]Pharmacokinetic parameters were calculated from plasma concentration–time data and are reported as mean values (n= 2–3 male Wistar-Han rats/dosing route). See supplemental information for additional details. [f] Oral pharmacokinetics studies were conducted in the fed state. Oral bioavailability (F) is defined as the dose-normalized AUC after oral administration divided by the dose-normalized AUC after intravenous administration. [g]Crystalline **6** was orally administered in anhydrous (Form 1) as well as anhydrous methyl-tert-butyl ether co-solvate form. [h]The fraction of the oral dose absorbed from the gastrointestinal tract (F_a x F_g) was estimated using the equation F_a x F_g = $F/(1 - CL_{blood}/Q)$ (*27*) (see supplemental section for additional details).

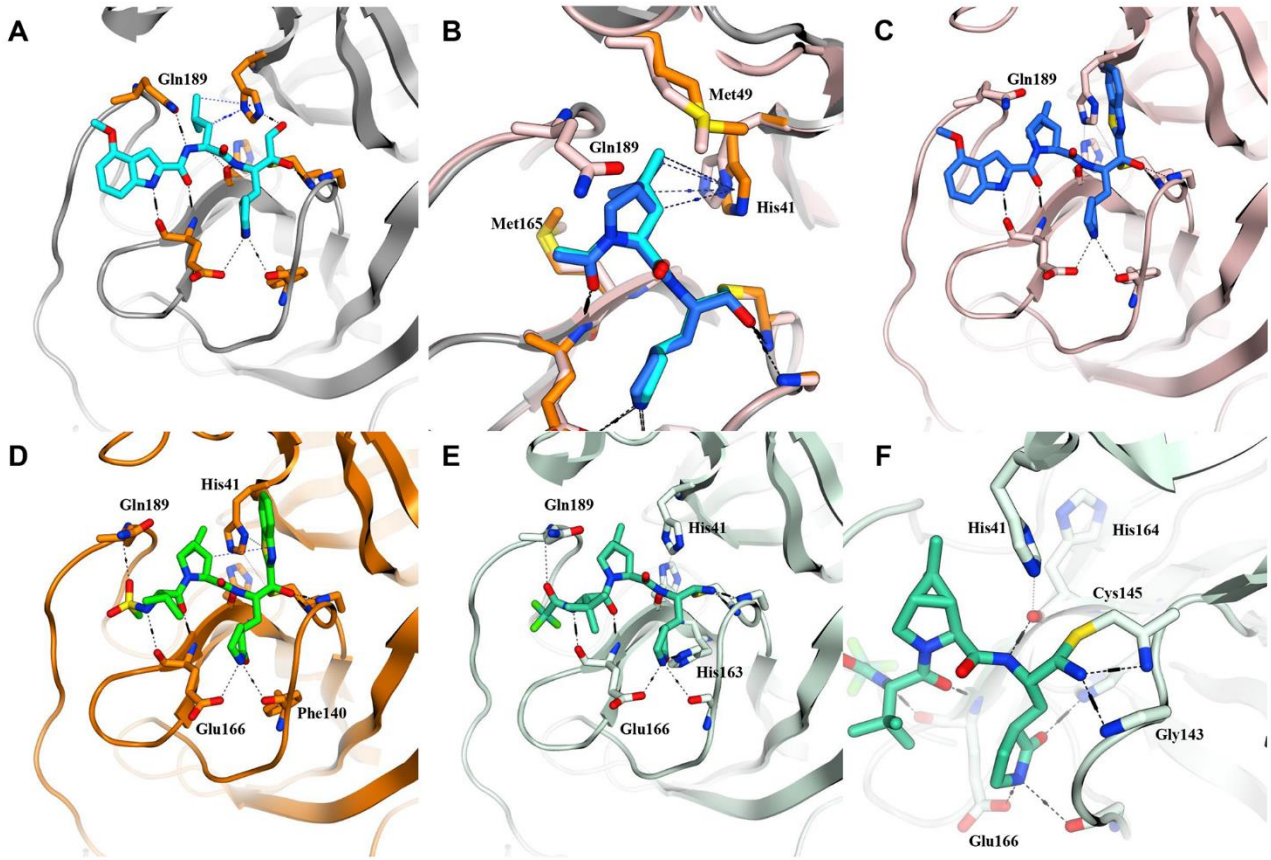

Fig. 2. SARS-CoV-2 M^{pro} structural biology. (**A**) Co-crystal structure of PF-00835231 (**1**) with SARS-CoV-2 M^{pro}. Key interactions are indicated. (**B**) Modeled overlap of dimethyl-bicyclo[3.1.0] proline from compound **3** (blue) as a mimic of P2 leucine residue (cyan) found in the viral polyprotein substrate and **1**. This tolerated P2 change eliminates an H-bond donor from resulting inhibitors. (**C**) Compound **3** effectively fills the lipophilic S2 pocket formed by Met49, Met165, and His41 but productive hydrogen bonding to Gln189 is no longer possible. (**D**) Compound **4** with optimized acyclic P3 group and restored Gln189 interaction. (**E**) SARS-CoV-2 M^{pro} bound crystal structure of clinical candidate PF-07321332 (**6**). (**F**) A reversible covalent Cys145 adduct is formed with the nitrile substituent in compound **6**.

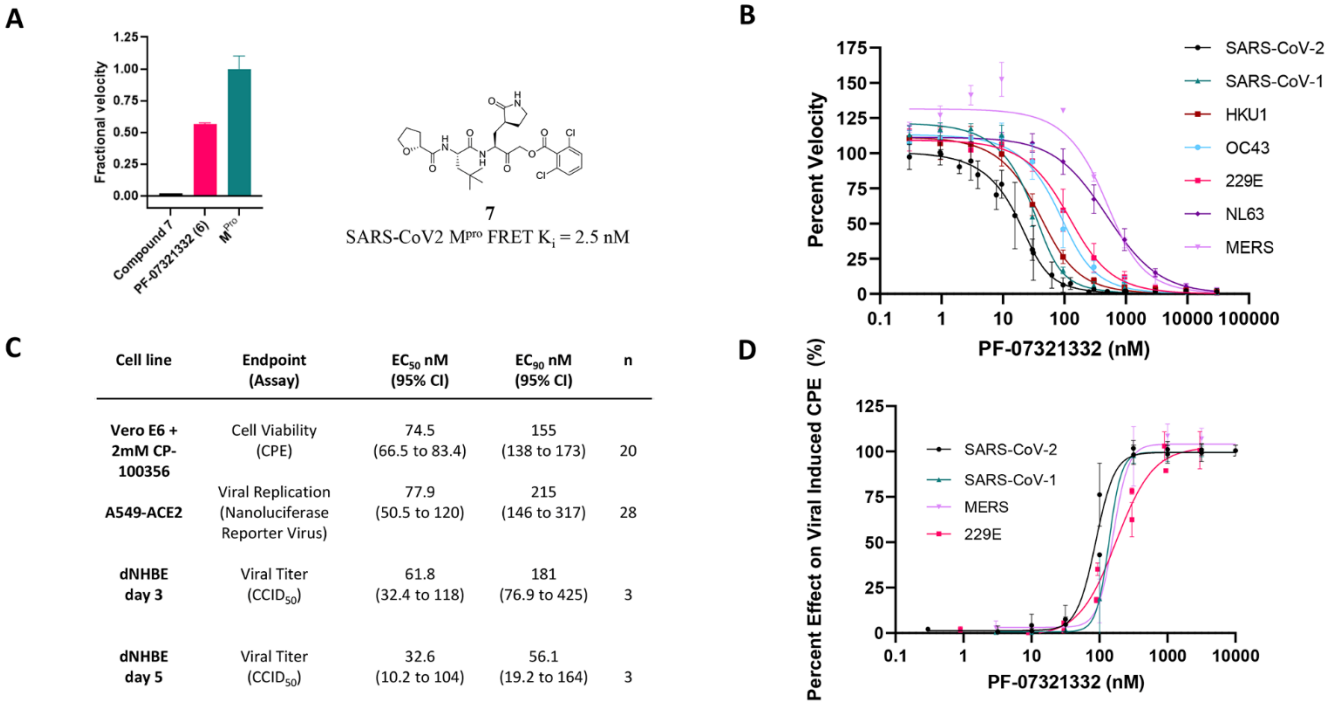

Cell line	Endpoint (Assay)	EC_{50} nM (95% CI)	EC_{90} nM (95% CI)	n
Vero E6 + 2mM CP-100356	Cell Viability (CPE)	74.5 (66.5 to 83.4)	155 (138 to 173)	20
A549-ACE2	Viral Replication (Nanoluciferase Reporter Virus)	77.9 (50.5 to 120)	215 (146 to 317)	28
dNHBE day 3	Viral Titer ($CCID_{50}$)	61.8 (32.4 to 118)	181 (76.9 to 425)	3
dNHBE day 5	Viral Titer ($CCID_{50}$)	32.6 (10.2 to 104)	56.1 (19.2 to 164)	3

Fig. 3. PF-07321332 biochemical and antiviral activity. (**A**) PF-07321332 is a reversible inhibitor of SARS-CoV-2 M^{pro} as demonstrated by recovery of enzymatic activity following a 100-fold dilution of the enzyme inhibitor complex. Compound **7** (PF-00956378), an irreversible inhibitor, was included as a control. Data are representative of 3 independent experiments. (**B**) PF-07321332 is a potent inhibitor of the proteolytic activity of SARS-CoV-2 M^{pro} as well as related coronaviruses in FRET assays. Data shown are the mean ± SD from 3 independent experiments. (**C**) PF-07321332 demonstrates potent SARS-CoV-2 antiviral cellular activity. PF-07321332 inhibited SARS-CoV-2 induced cytopathic effect (CPE) in Vero E6 cells enriched for ACE2. A P-glycoprotein inhibitor, CP-100356 (efflux inhibitor, EI) was added at 2 μM to inhibit the P-glycoprotein mediated efflux of PF-07321332. In Vero E6 cells with no EI, the EC_{50} of PF-07321332 (95% confidence interval (CI)) was 4.48 μM (3.55 to 5.65 μM) (N=8, n=20). Cytotoxicity of PF-07321332 was evaluated in non-infected cells and the CC_{50} was >100 μM (table S4). PF-07321332 inhibits SARS-CoV-2 replication in A549 cells expressing ACE2 in 4 independent experiments. The CC_{50} in non-infected A549 cells was >3 μM (table S4). In differentiated normal human bronchial epithelial (dNHBE) cells, PF-07321332 decreased SARS-CoV-2 viral replication (N=3). Data shown are the geometric mean and 95% confidence intervals (CI). (**D**) PF-07321332 demonstrates pancoronavirus antiviral activity. PF-07321332 inhibition in viral-induced CPE assays: SARS-CoV-1 in Vero E6 cells (in the presence of 2 μM EI CP-100356), h-CoV-229E in MRC-5 cells and MERS in Vero 81 cells (in the presence of 1 μM EI CP-100356). Data shown are the mean and SD. CC_{50} values determined in all assays to be >100 μM (table S4).

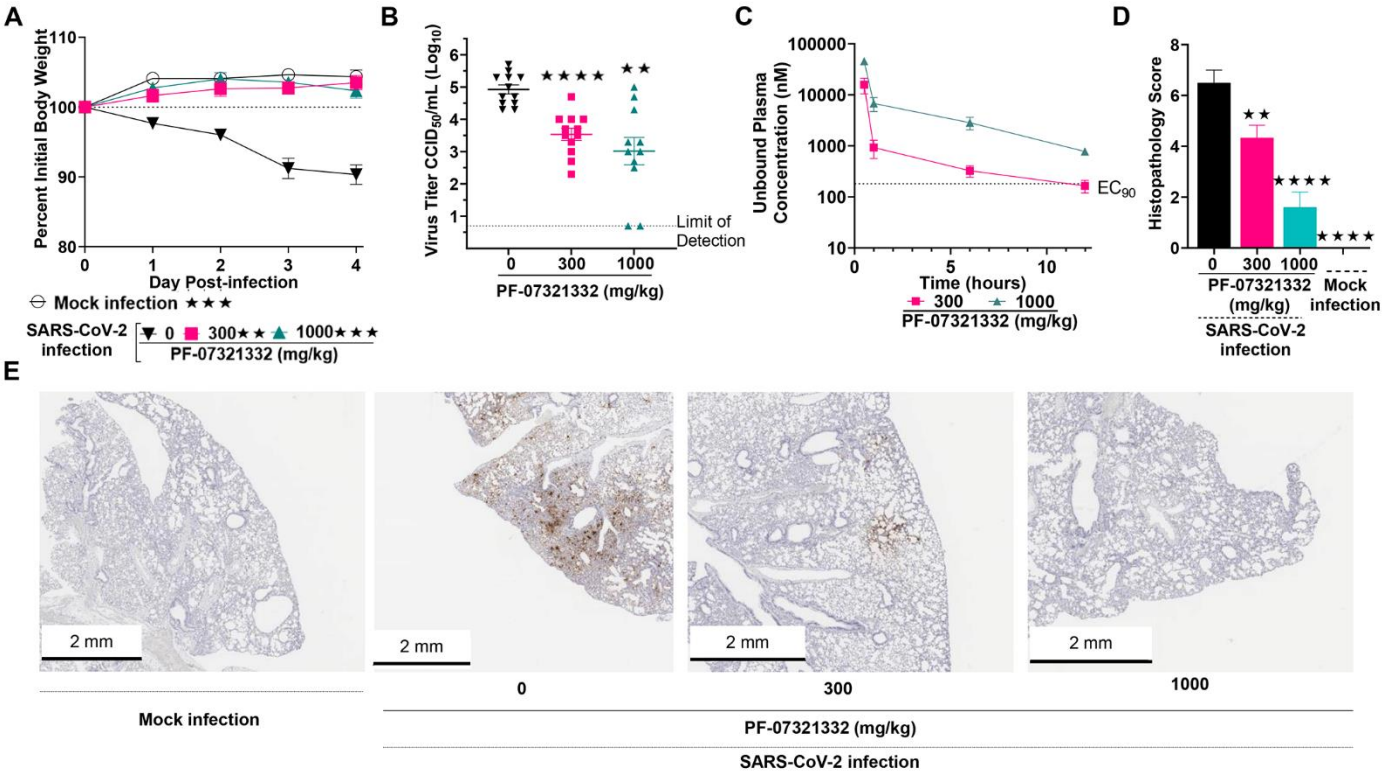

Fig. 4. In vivo efficacy of PF-07321332 against SARS-CoV-2 MA10 infection in mice. Six-mice/group were challenged intranasally with $1 \times 10^{5.0}$ 50% cell culture infectious doses of SARS-CoV-2 MA10 ($CCID_{50}$). Animals were orally administered 300 or 1000 mg/kg PF-07321332 or vehicle (placebo) twice daily (BID) at 4 hours post-infection. Animals were euthanized at 4 days post infection (dpi) and lungs collected for virus titers. Data for A-D are compiled from two independent studies (n=12, BALB/c mice). (**A**) Weight loss during infection. Mice were weighed daily. (**B**) Lung viral titer at 4 dpi. Lung titers are graphed as mean Log_{10} $CCID_{50}$/ml +/− std error of mean. Dotted line represents the limit of detection for the $CCID_{50}$ assay. (**C**) 12-hour PF-07321332 exposure levels of 300 and 1000mg/kg doses in uninfected, orally treated mice. EC_{90} represented as determined in the day 3 dNHBE primary cell assay (**D**) Histopathology scores on a scale of 0-5 where 0 is a normal healthy lung and 5 is severe coalescing areas of necrosis and confluent areas of inflammation. (**E**) SARS-CoV-2 Nucleocapsid Protein immunohistochemistry. Digital light microscopic scans of mouse lung tissue sections of mock-infected, placebo, 300 mg/kg PF-07321332, and 1000 mg/kg PF-07321332 treated mice stained with SARS-CoV-2 Nucleocapsid antibody. Data are scans from one study. The scale bars represent 2mm. Magnification shown is 1x.

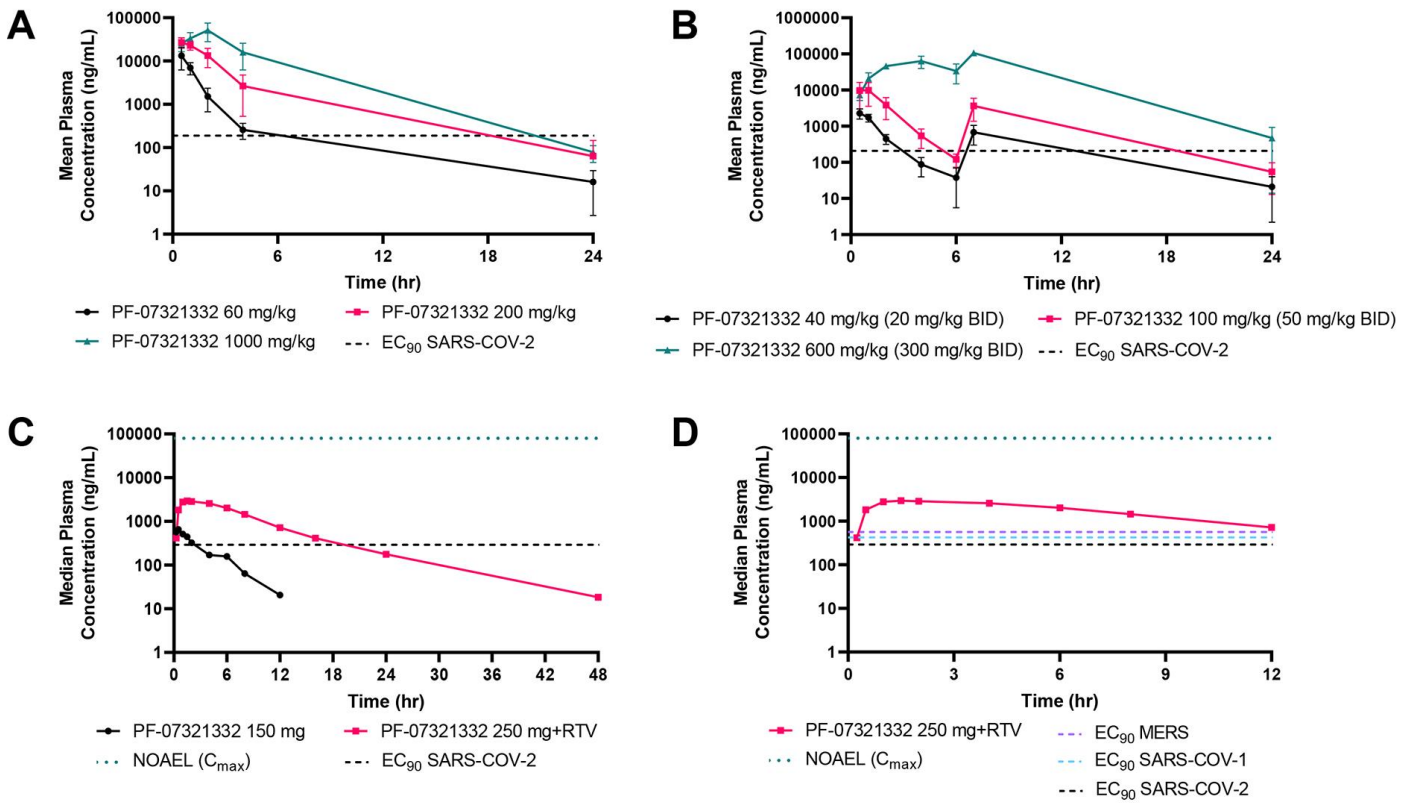

Fig. 5. Preclinical toxicology and healthy adult participant single ascending dose study exposures for PF-07321332. (**A**) Rat oral toxicokinetic exposures (day 14) of once-daily administered PF-07321332 compared with day 3 antiviral EC_{90} values in dNHBE cells. (**B**) Monkey oral toxicokinetic exposures (day 15) of twice-daily administered PF-07321332 compared with day 3 antiviral EC_{90} in dNHBE. (**C**) Human plasma concentrations (total) versus time profile after oral administration (fasted state) of PF-07321332 (150 mg) and PF-07321332 (250 mg) with ritonavir (RTV) (100 mg at t = -12 hours, 0 hours and 12 hours) compared with day 3 antiviral EC_{90} in dNHBE. (**D**) Human antiviral target coverage >$EC_{90,u}$ at 12 hours for SARS-CoV-1, SARS-CoV-2 and MERS post oral administration of PF-07321332 (250 mg) and ritonavir (100 mg at t = -12 hours, 0 hours and 12 hours). The in vitro unbound SARS-COV-2 EC_{90} of 181 nM was converted to ng/ml using a molecular weight of 499.5 g/mol for PF-07321332. Total EC_{90} was calculated by dividing unbound EC_{90} by $f_{u,plasma}$ (rat 0.479, NHP 0.208, and human 0.310). This resulted in total EC_{90} values of 189, 208, and 292 ng/ml for rat, NHP, and human, respectively. The calculated total human EC_{90} for MERS and SARS-COV-1 were 566 and 422 ng/ml, respectively. A human NOAEL of 79,700 ng/ml (for C_{max}) was estimated from the rat C_{max} value of 51500 ng/ml at the NOAEL dose of 1000 mg/kg, normalizing for plasma unbound fraction differences.

An oral SARS-CoV-2 M inhibitor clinical candidate for the treatment of COVID-19

Dafydd R. OwenCharlotte M. N. AllertonAnnaliesa S. AndersonLisa AschenbrennerMelissa AverySimon BerrittBritton BorasRhonda D. CardinAnthony CarloKaren J. CoffmanAlyssa DantonioLi DiHeather EngRoseAnn FerreKetan S. GajiwalaScott A. GibsonSamantha E. GreasleyBrett L. HurstEugene P. KadarAmit S. KalgutkarJack C. LeeJisun LeeWei LiuStephen W. MasonStephen NoellJonathan J. NovakR. Scott ObachKevin OgilvieNandini C. PatelMartin PetterssonDevendra K. RaiMatthew R. ReeseMatthew F. SammonsJean G. SathishRavi Shankar P. SinghClaire M. SteppanAl E. StewartJamison B. TuttleLawrence UpdykePatrick R. VerhoestLiuqing WeiQingyi YangYuao Zhu

Science, **Ahead of Print** • DOI: 10.1126/science.abl4784